# Study of thermal hydraulic characteristics of a pebble bed reactor using computational fluid dynamics

**MA Xinrui[1], PENG Minjun[1], WANG Chengqi[1], and YU Dali[1]**

1. *Foundational Science on Nuclear Safety and Simulation Laboratory, Harbin Engineering University, Harbin 150001, P.R. China. (mxr198708@163.com)*

**Abstract**: This research investigates the thermal hydraulic characteristics of a Pebble Bed Reactor (PBR) core with different pebble diameters using commercial software CFX. The coolant is water. A "Bridge" model is employed to simplify the contact points; the standard $k-\varepsilon$ model is adopted to simulate flow turbulence. Velocity and temperature fields as well as Nusselt number are obtained and analyzed under different pebble sizes; the influence of pebble size on flow and heat transfer is also discussed. Then, the well-known KTA correlation is adopted to validate the simulation results. The results show that different pebble diameters do not change the flow distribution significantly. Four areas with low temperature appear at the four pore regions and four pairs of eddies at the intervals of the upper and lower bridges both impact the thermal hydraulic characteristics distribution. In addition, the maximum temperature increases and pressure drop decreases with the enlarging of pebble diameters. The study could provide the basis for further experimental research and design improvement of fuel spheres in PBR.

**Keywords**: pebble bed reactor; thermal hydraulic characteristics; CFD

## 1 Introduction

For pebble fuel research, most efforts have been concentrated on High Temperature Gas-Cooled Reactors. If water is selected as the coolant, it can combine the advantages of a traditional pressurized water reactor and pebble bed reactor (PBR). Since experimental data of this type of reactor is extremely scarce, accurate numerical simulations of thermal hydraulic characteristics in the core are desired to investigate the safety performance and provide a basis for conducting further experimental research.

Due to the complexity and limitations of experimental research, computational fluid dynamics (CFD) has been adopted by many researchers to study thermal hydraulics characteristics of PBR. For instance, Guardo *et al*. [1] analyzed the performance of five different turbulence models on particle-to-fluid heat transfer in a fixed bed; Ferng and Lin [2] investigated the effect of two typical pebble arrangements—body-centered cubic (BCC) and Face-centered cubic (FCC)—on thermal hydraulic characteristics.

One main problem of CFD investigation of pebble beds is how to create high-quality meshes near contact points. Therefore, effective simplifications or modifications on contact points, which can improve simulation efficiency without sacrificing accuracy, are valuable, especially when the geometry of the pebble bed is highly complicated, for example, a random arranged pebble bed. Based on this consideration, different numerical treatments on contact points have been presented. Nijemeisland and Dixon [3] proposed to shrink the fuel pebbles by a certain amount, thus a small gap was left between two adjacent pebbles (gap model). By contrast, Guardo *et al*. [4] increased the pebble diameter, therefore two neighboring pebbles overlapped each other by a certain amount, forming area contact (overlap model). Eppinger *et al*. [5] flattened the pebbles near contact points locally (cap model). The performance of these modifications was tested by other researchers. Jung-Jae Lee *et al*. [6], Dixon *et al*. [7] compared the four modifications comprehensively. Ookawara *et al*. [8] replaced the contact point with a small cylindrical bridge whose axis lies on a line connecting the particle centers (bridge model). Among all the treatments of contact points, the bridge model was considered to provide the minimum change to the porosity. Besides, it is anticipated that in practice the pebble would produce a small deformation and form a tiny contact surface due to gravity, and the bridge model could simulate this phenomenon better, therefore the bridge model is

**Received date: November 18, 2015**
(Revised date: December 11, 2015)

applied prior to other methods. A consensus was also formed that the bridge model would give the most reasonable simulation results in velocity, temperature and Nusselt number ( $Nu$ ) compared with the other three models.

In this present research, the bridge model is employed to examine the flow and heat transfer in a pebble bed with different pebble diameters. A volume heat source was adopted and water is used as the coolant according to the parameters of the Atoms for Peace Reactor (AFPR), presented by Pacific Northwest National Laboratory (PNNL)[9]. AFPR is a water-cooled fixed particle bed reactor whose fuel has similar design requirements with the fuel pebbles tested in this paper. In accordance with the AFPR report, the pebble outer diameter size varies from 10-15**mm.** In the PBR thermodynamic system the coolant in the core will undergo multiple thermodynamic processes and the thermal hydraulic characteristics are considerably complex, therefore different diameter sizes probably impact the flow and heat transfer capability in the PBR. Thus, it is necessary to investigate this issue.

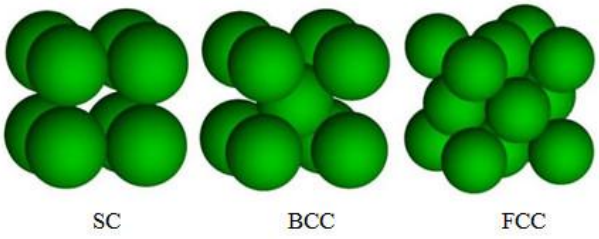


Fig.1 Three kinds of pebble arrangements.

# 2 Model setup and analysis

## 2.1 Physical model

It is not easy to model a unique random arrangement for pebbles. Generally, most of the simulations assume a fixed arrangement of pebbles, which includes three types of arrangements: simple cubic (SC), BCC and FCC. A realistic pebble arrangement is a combination of different structured arrangements. The structures of the three arrangements are presented in Fig.1. The porosity ratios of the three arrangements are 0.4764, 0.3198, and 0.2595 respectively. The porosity of BCC is closest to that of a random packed pebble bed whose porosity ratio varies from 0.36 to 0.41. The SC arrangement is difficult to realize in an actual project and the overall heat transfer performance of FCC arrangement is lower than BCC packing. Therefore, the BCC arrangement was selected in this study.

Following the design concept of AFPR, the spherical cermet fuel used in this article consists of coated $UO_2$ kernels embedded in a zirconium matrix which is then overcoated with a protective Zr-outer coating (as shown in Fig.2). Thus different materials are used for the kernel and coat of fuel spheres in this simulation. Fig.3 (a) and (b) present the structure of the whole simulation geometry and the fluid domain, respectively. In order to eliminate the influence of the outlet flow, an extra flow length was added to the last layer of the pebbles. Fig.4 displays the structure of solid domains which consist of 7 layers of pebbles.

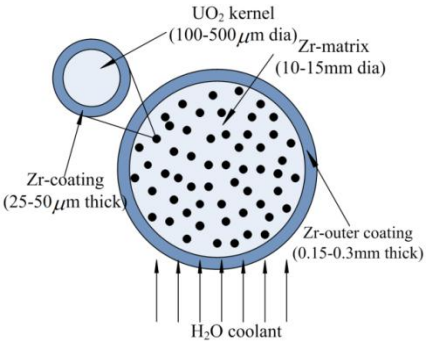


Fig.2. Structure of the cermet fuel.

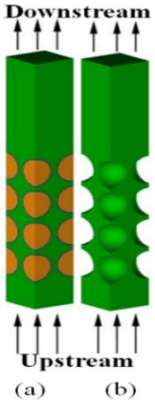


Fig.3. Structure of geometry and fluid domain.

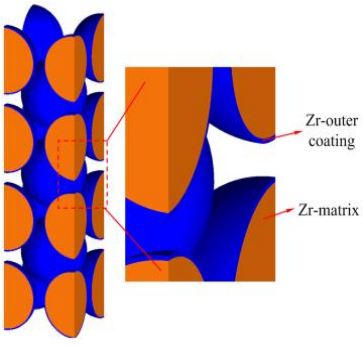


Fig.4. Structure of the solid domain.

In this article, the bridge model is adopted to simplify the contact points by replacing contact points with small cylinders. The details of the bridge model are presented in Fig.5. The diameter of the cylinder ($\phi$) is 12% of the pebble diameter ($d$).

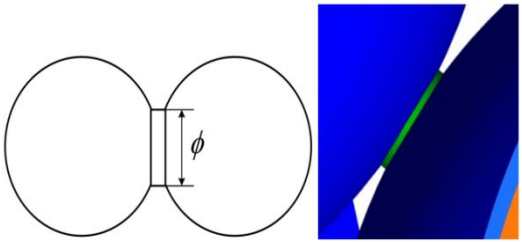


Fig.5. Details of bridge model.

**2.2 Mathematical model**

2.2.1 Governing equations

For the Zr-matrix domain, the simplified one-dimensional mathematical equation for heat conduction with heat sources can be written as:

$$\frac{1}{r^2}\frac{dT(r)}{dr}(k_m r^2\frac{dT(r)}{dr})+q'''=0 \quad (2.1)$$

The simplified one-dimensional mathematical equation for heat conduction in Zr-outer coatings without heat sources can be written as:

$$\frac{1}{r^2}\frac{dT(r)}{dr}(k_c r^2\frac{dT(r)}{dr})=0 \quad (2.2)$$

where $k_m$ / $k_c$ is the thermal conductivity of Zr-matrix/ Zr-outer coatings; $q'''$ is the heat production per unit volume of the matrix; $T(r)$ is temperature of concerned position; $r$ is the distance from the center of the pebble.

Given that the temperature rise of the coolant from inlet to outlet is small, the physical property changes of water are neglected. Based on this assumption, the governing equations of the fluid domain can be written as follows:

Continuity equation:

$$\frac{\partial u}{\partial x}+\frac{\partial v}{\partial y}+\frac{\partial w}{\partial z}=0 \quad (2.3)$$

Momentum equation:

$$\rho(\frac{\partial U}{\partial \tau}+u\frac{\partial U}{\partial x}+v\frac{\partial U}{\partial y}+w\frac{\partial U}{\partial z})=F_P-\frac{\partial P}{\partial z}+\eta(\frac{\partial^2 U}{\partial x^2}+\frac{\partial^2 U}{\partial y^2}+\frac{\partial^2 U}{\partial z^2}) \quad (2.4)$$

Energy equation:

$$\frac{\partial T}{\partial \tau}+u\frac{\partial T}{\partial x}+v\frac{\partial T}{\partial y}+w\frac{\partial T}{\partial z}=\frac{\lambda}{\rho c_P}(\frac{\partial^2 T}{\partial x^2}+\frac{\partial^2 T}{\partial y^2}+\frac{\partial^2 T}{\partial z^2}) \quad (2.5)$$

where $U$ is internal energy.

2.2.2 Selection of the turbulence model

The standard $k-\varepsilon$ is adopted to close the governing equations. It is a mature and effective model for this type of problem regardless of whether the Reynolds number is high or low. $k$ is the turbulence kinetic energy and is defined as the variance of the fluctuations in velocity. $\varepsilon$ is the turbulence eddy dissipation. The $k-\varepsilon$ model introduces two variables into the system of equations. The continuity equation is then:

$$\frac{\partial \rho}{\partial t}+\frac{\partial}{\partial x_j}(\rho U_j)=0 \quad (2.6)$$

And the momentum equation becomes:

$$\frac{\partial \rho U_i}{\partial t}+\frac{\partial}{\partial x_j}(\rho U_i U_j)=-\frac{\partial p'}{\partial x_i}+\frac{\partial}{\partial x_j}\left[\mu_{eff}(\frac{\partial U_i}{\partial x_i}+\frac{\partial U_j}{\partial x_j})\right]+S_M \quad (2.7)$$

where $S_M$ is the sum of body forces, $\mu_{eff}$ is the effective viscosity accounting for turbulence, and $p'$ is the modified pressure as defined by:

$$p'=p+\frac{2}{3}\rho k+\frac{2}{3}\mu_{eff}\frac{\partial U_k}{\partial x_k} \quad (2.8)$$

The $k-\varepsilon$ model, like the zero equation model, is based on the eddy viscosity concept, so that:

$$\mu_{eff}=\mu+\mu_t \quad (2.9)$$

where $\mu_t$ is the turbulence viscosity. The $k-\varepsilon$ model assumes that the turbulence viscosity is linked to the turbulence kinetic energy and dissipation via the relation:

$$\mu_t=C_\mu\rho\frac{k^2}{\varepsilon} \quad (2.10)$$

where $C_\mu$ is a constant, having the value of 0.09. The value of $k$ and $\varepsilon$ come directly from the differential transport equations for the turbulence kinetic energy and turbulence dissipation rate:

$$\frac{\partial(\rho k)}{\partial t}+\frac{\partial}{\partial x_j}(\rho U_j k)=\frac{\partial}{\partial x_j}\left[(\mu+\frac{\mu_t}{\sigma_k})\frac{\partial k}{\partial x_j}\right]+P_k-\rho\varepsilon \quad (2.11)$$

$$\frac{\partial(\varepsilon k)}{\partial t}+\frac{\partial}{\partial x_j}(\rho U_j \varepsilon)=\frac{\partial}{\partial x_j}\left[(\mu+\frac{\mu_t}{\sigma_\varepsilon})\frac{\partial \varepsilon}{\partial x_j}\right]+\frac{\varepsilon}{k}(C_{\varepsilon 1}P_k-C_{\varepsilon 2}\rho\varepsilon) \quad (2.12)$$

where $C_{\varepsilon 1}$, $C_{\varepsilon 2}$, $\sigma_k$ and $\sigma_\varepsilon$ are constants with the value of 1.44, 1.92, 1.0 and 1.3, respectively.

# 3 Numerical simulations

## 3.1 Computational grids

An unstructured mesh is applied in the fluid domain, three layers of prism meshes are created on the interface of solid to fluid to keep y+ near the wall under the value of 40 (As shown in Fig.6 (a)). For Zr-outer coating and Zr-matrix, a structured mesh is adopted to increase the simulation accuracy. The unstructured meshes in the fluid domain are refined at narrow regions (As shown in Fig.6 (b)).

Mesh independent calculations are performed with $d$ =10**mm**, using different mesh sizes (as shown in Table 1), to make sure the simulation results are mesh independent. The pebble diameter used in AFPR is 10-15**mm**, thus the classification of cases investigated in this research is 10**mm**, 13**mm** and 16mm respectively as per Table 2.

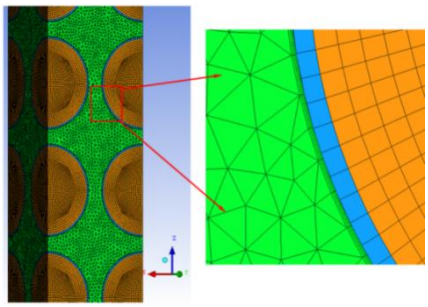

(a)prism meshes

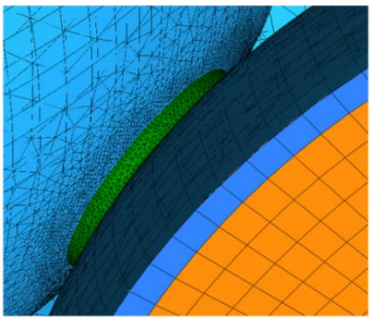

(b) Locally refined meshes

Fig.6. Meshes in three domains.

**Table.1. Different mesh sizes in mesh independent calculations**

| Case name | Scale factor | Maximum element | The quantity of meshes |
|---|---|---|---|
| Size A | 1.2 | 0.65 | 2,139,834 |
| Size B | 1.1 | 0.65 | 3,044,751 |
| Size C | 1.05 | 0.65 | 3,695,466 |

**Table.2. Classification of cases investigated**

| Case name | Pebble diameter | Coating thickness |
|---|---|---|
| A | 10mm | 0.20mm |
| B | 13mm | 0.26mm |
| C | 16mm | 0.32mm |

**Table.3 Parameters used in this investigation**

| Parameters | Value | Unit |
|---|---|---|
| Inlet temperature | 573.15 | K |
| Outlet pressure | 12.41 | MPa |
| Inlet normal speed | 0.1104 | m/s |
| Water density | $720.40^{3}$ | kg/m |
| Specific heat capacity of water | 5575.34 | $J/kg^{-1}K^{-1}$ |
| Kinematic viscosity | $8.970^{-6}$ | Pa/s |
| Heat conduction coefficient of coolant | 0.5538 | $Wm^{-1}K^{-1}$ |
| Specific heat capacity of coatings | 298.75 | $J/kg^{-1}K^{-1}$ |
| Heat conduction coefficient of coating | 20.5 | $Wm^{-1}K^{-1}$ |
| Specific heat capacity of matrix | 296.0 | J/kg-1K-1 |
| Heat conduction coefficient of matrix | 15.6 | Wm-1K-1 |
| Heat production in matrix | 59.727 | $MW/m^{3}$ |

### 3.2 Boundary conditions

The boundary conditions of this research are based on the design parameters of AFPR. The inlet temperature of coolant is 573.15**K**; the normal speed of inlet flow is 0.1104 **m/s** with a turbulence intensity of 5%. Opening condition is applied to outlet with pressure of 12.41**MPa**. Symmetrical conditions are used at the four vertical surfaces. Volume heat source of 59.727**MW/m**$^3$ is applied to Zr-matrix. All these parameters as well as other necessary information are listed in Table.3.

## 4 Results analysis and verification

### 4.1 Results analysis

Fig.7 shows the temperature distribution on the central full pebble surface. The corresponding velocity and pressure distributions are displayed in Fig.8 and Fig.9, respectively. The different colors indicate the magnitude of different values. It can be seen that the distributions of the three parameters are similar for different pebble diameters. High temperature appears at the top of the pebble surface facing the upstream direction. Four areas with low temperature form at the pore regions. In addition, the temperature near contact zones is relatively higher than neighboring regions. Furthermore, Fig.7, Fig.8 and Fig.9 show good agreement with each other in general, following the pattern that: (a) low temperature overlaps with high velocity since high velocity improves heat transfer; (b) high velocity overlaps with low pressure, which can be explained by the Bernoulli equation.

Although the distributions trend of the three parameters is similar in general, they differ in specific values. With the increase of pebble diameters, the maximum velocity on the pebble surface decreases while the maximum temperature increases. This could be explained by the heat generated by the fuel which is in direct proportion to pebble volume, which makes the temperature increase and the heat transferred between fuel and coolant that is relative to pebble area makes temperature decrease, therefore, the pebble temperature is only associated with pebble diameter when all the other conditions are the same. Additionally, according to calculation results, the average velocity on the pebble surface for cases A, B and C are 0.289m/s, 0.288m/s and 0.286m/s, respectively, which also decreases with the increase of pebble diameters, although the distinction is very small. Because the pressure drops of the three cases are negligible compared to the operation pressure, the distinctions of pressure drop for the three cases cannot be expressed clearly by Fig.9.

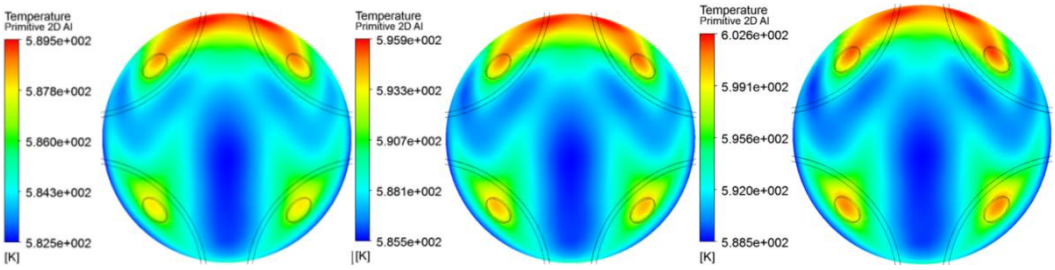


(a) Case A (b) Case B (c) Case C

Fig.7. Distribution of temperature on pebble surface (view from +Y).

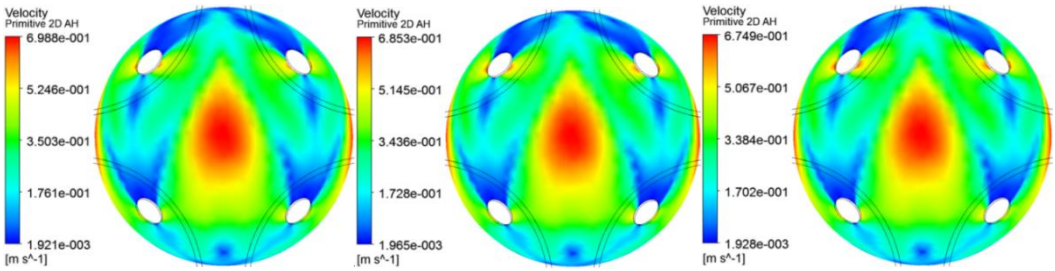


(a) Case A (b) Case B (c) Case C

Fig.8. Distribution of coolant velocity on pebble surface (view from +Y).

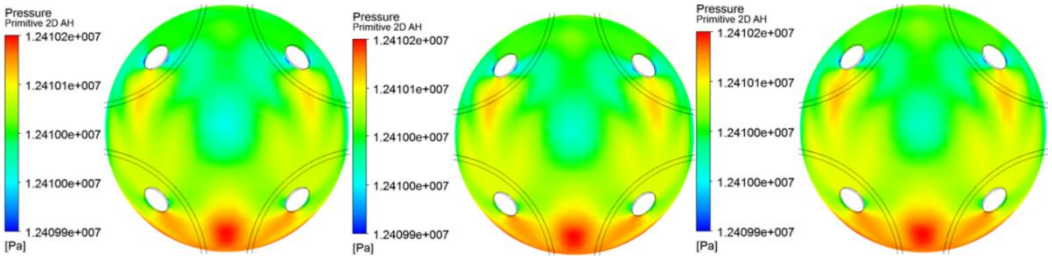


(a) Case A (b) Case B (c) Case C

Fig.9. Distribution of pressure on pebble surface (view from +Y).

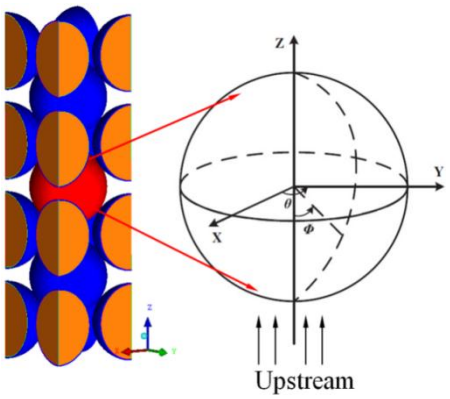


Fig.10. Definition of $\theta$ and $\Phi$.

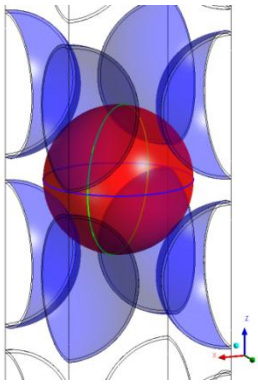

Fig.11. Positions of data sources.

In order to express the results of the simulation quantitatively, two angles, $\theta$ and $\Phi$, are defined (as shown in Fig.10); the data along two circles (as shown in Fig.11) on the pebble surface are extracted individually. Circle 1 (the green circle in Fig.11) crosses two upper diagonal gaps/bridges, two lower diagonal gaps/bridges, the top point and the bottom point of the pebble surface. Circle 2 (the blue circle in Fig.11) is the equator of the central full pebble.

Fig.12, Fig.13 and Fig.14 display the distributions of temperature, velocity and $Nu$ along circle 1, respectively. The dotted lines indicate the positions of bridges. It can be observed that there are two temperature peaks located at the lower and upper bridge. But the second peak is not obvious because it has a similar value to the posterior temperature. In addition, the temperature along circle 1 increases with the increasing pebble diameters. Furthermore the change of temperature along circle 1 for the larger pebble is also more drastic. However, the distributions of velocity and $Nu$ for the three cases are almost the same.

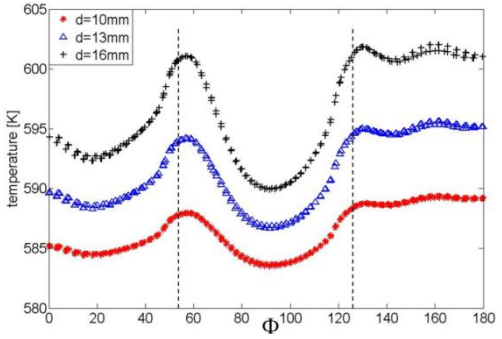


Fig.12. Temperature distributions along circle 1.

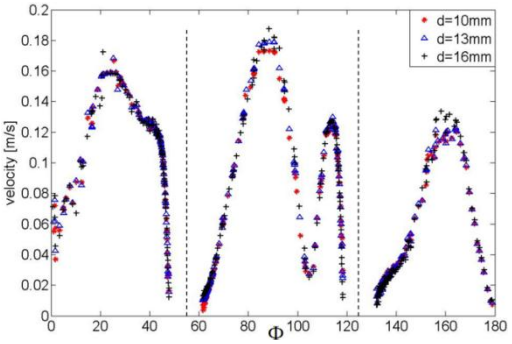


Fig.13. Velocity distributions along circle 1.

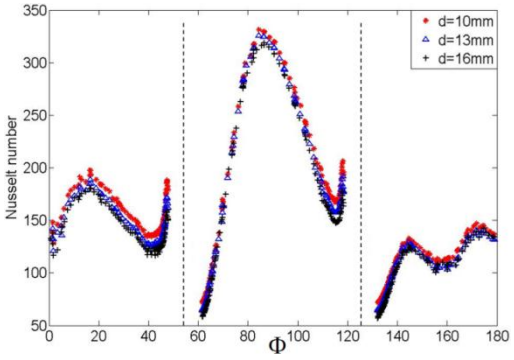


Fig.14. Nusselt number distributions along circle 1.

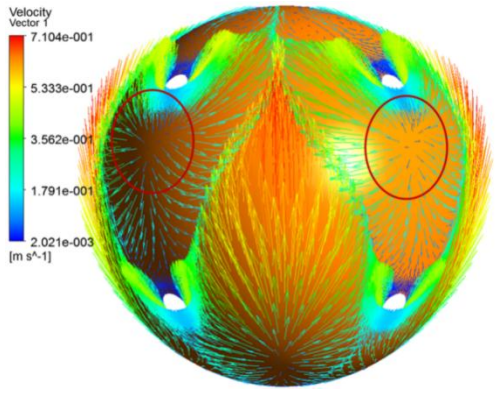


Fig.15. Velocity vectors on pebble surface (view from +Y, Case A)

In Fig.13, it can be observed that the velocity at the front of the bridges drops sharply due to the resistance caused by the bridges. Furthermore, the coolant flows around bridges, which leads to extremely low velocity at the back of the bridges ($\Phi$ =60 °, 160 °). An extra dip in velocity can be found when $\Phi$ =105 ° in Fig.13. This phenomenon can be explained by velocity vectors on the pebble surface. It can be clearly found the water flow stagnates at regions surrounded by red circles (as shown in Fig.15). Part of the coolant flows downward and part of it flows upward, which leads to the sharp changes of velocity at $\Phi$ =105 °. But in general, the velocity distribution is consistent with the $Nu$ distribution (Fig.14) following the discipline that $Nu$ increases/ decreases with the increasing/decreasing of velocity. The relatively higher value of $Nu$ at the front of bridges can be attributed to the flow scouring in this area.

The distributions of temperature, velocity and $Nu$ along line 2 are shown in Fig.16, Fig.17 and Fig.18, respectively. The maximum velocities appear at $\theta$ =0, 90 °, 180 °, 270 ° which lead to minimum temperatures at these positions. The minimum velocities are located at $\theta$ =45 °, 135 °, 225 °, 315 ° which is the interval between upper bridges and lower bridges. However, the maximum $Nu$ is also located at these positions and the temperature is lower than neighboring positions. This phenomenon indicates stronger local turbulence which can be confirmed by Fig.19, taking Case A as an example. Four pairs of eddies form at these positions, which serve as mixing forces that improve heat transfer. In addition, the distributions of velocity and $Nu$ are almost the same for different pebble diameters.

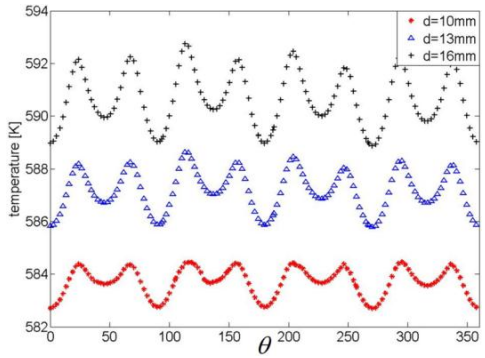


Fig.16. Temperature distributions along circle 2.

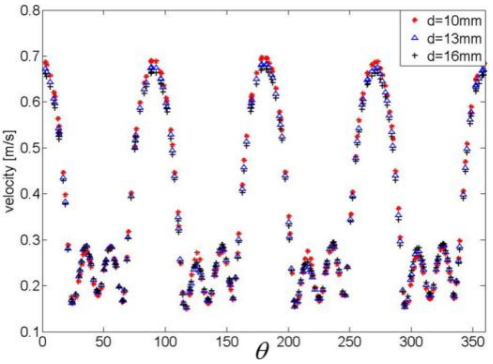


Fig.17. Velocity distributions along circle 2.

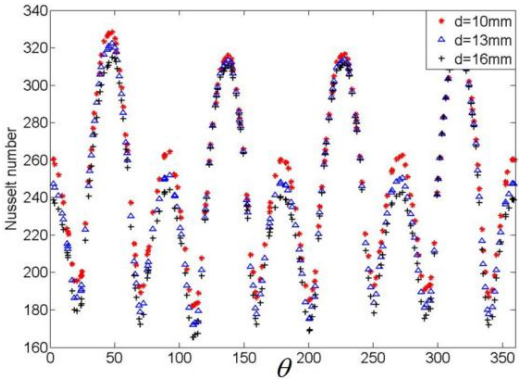


Fig.18. Nusselt number distributions along circle 2.

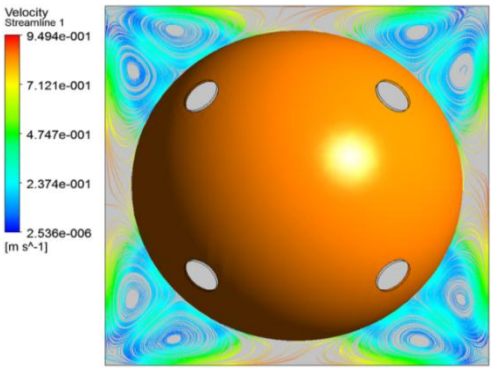


Fig.19. Eddies at corners of fluid domain. (Case A, view from +Z).

In order to express the influence of pebble diameter on the temperature in pebbles, the distributions of temperature along two lines (as shown in Fig.20) are displayed in Fig.21 and Fig.22. Line one (the green

one in Fig.20) is parallel to X-axis while line 2 (the red one in Fig.20) is parallel to Z-axis and both of them cross the center of the pebble. As indicated by Fig.21, the temperature in pebble fuel increases drastically with the increasing pebble diameter. Furthermore, the horizontal temperature distribution is symmetrical to the central point (as shown in Fig.21) while the temperature of the upper hemisphere is obviously higher than that of the lower part (as shown in Fig.22) because the coolant from upstream strikes the lower part of pebble surface while it detaches from pebble surface at the higher part, which leads to different heat transfer conditions.

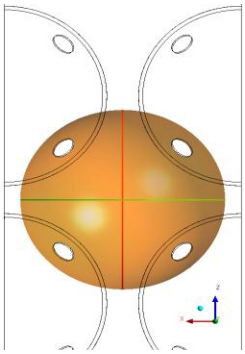

Fig.20. Positions of two lines in the central full pebble.

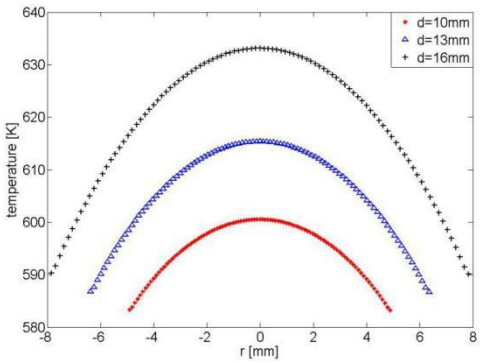


Fig.21. Temperature distributions along line 1.

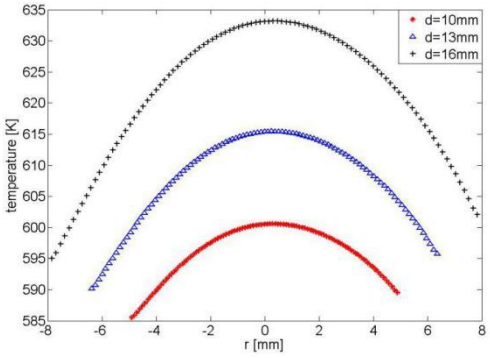


Fig.22. Temperature distributions along line 2.

### 4.2 Results verification

To validate the simulation results, the well-known KTA correlation is used to calculate the central temperature of each layer pebbles. The empirical KTA correlation is suitable for application to pebbles with porosity of 0.36–0.42. The KTA correlation can be described as follows:

$$Nu = 1.27\frac{\mathrm{Pr}^{1/3}}{\varepsilon_0^{1.18}}R\mathrm{e}^{0.36} + 0.033\frac{\mathrm{Pr}^{1/2}}{\varepsilon_0^{1.07}}R\mathrm{e}^{0.86} \qquad (4.1)$$

where Pr is the Prandtl number and $Re$ is the Reynolds number (Nuclear Safety Standards Commission (1983)[10]).

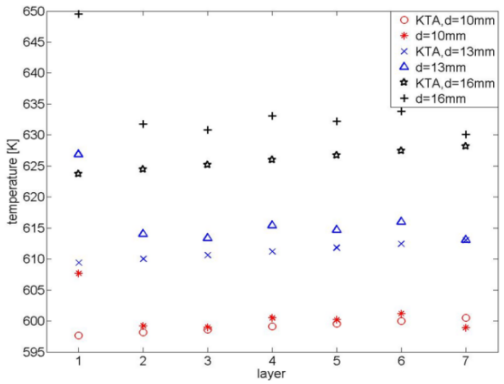


Fig.23. Comparisons with KTA.

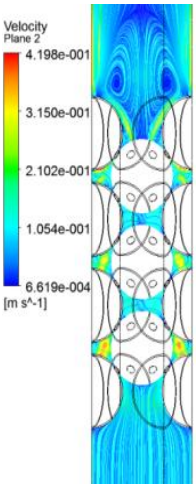


Fig.24. Streamlines at inlet and outlet (Case A).

The KTA correlation is one which is widely adopted for system codes to predict the heat transfer characteristics for pebble beds. The comparison between KTA and the present investigation is demonstrated in Fig.23. It can be seen that the central temperature predicted by this research is higher than results obtained from the KTA correlation. The center temperature of layer 1 is much higher because the inlet flow does not develop thoroughly until it comes to layer 2. The lower velocity and slighter turbulence at

inlet contribute to the higher center temperature. By contrast, the outlet flow lowers the center temperature of the last layer pebbles by forming eddies at the tails of the four quarter pebbles which can be seen in Fig.24. The center temperature increases along the flow direction generally although fluctuation exists, which indicates simulation domains consisting of more pebbles horizontally might be more appropriate.

## 5 Conclusions

The present research investigates the thermal hydraulic characteristics of water flow in a BCC structured pebble bed with different pebble diameters– 10mm, 13mm and 16mm. The real contact points between two neighboring pebbles are replaced by artificial cylindrical bridges which connect two adjacent pebbles. The temperature, velocity and pressure on the pebble surface are obtained and analyzed. The influence on thermal hydraulics of pebble diameters is carefully analyzed. The major conclusions are as follows:

(1) The different pebble diameters used in this investigation do not change the flow distribution in pebble bed significantly although there are obvious differences locally. Correspondingly, the heat transfer conditions are also similar for different pebble diameters. The central temperature increases by more than 30K when the diameter is enlarged from 10mm to 16mm. The maximum temperature at pebble surface rises with the increase of pebble diameter, but the distinction is no larger than 2K when the diameter is enlarged from 10mm to 16mm.

(2) Four areas with low temperature appear at the four pore regions and four pairs of eddies at the intervals of the upper and lower bridges both impact the thermal hydraulic characteristics distribution. The temperature distribution is mainly caused by the changes of flow velocity on the pebble surface, following the pattern that high velocity leads to low temperature. Furthermore, hot spots appear near the bridges, which are caused by flow detachment behind the bridge. The extremely low flow rate deteriorates heat transfer conditions locally.

(3) The maximum temperature at the pebble surface rises with the increase of pebble diameter, however, as the pressure drop along the reactor core is supposed to decrease with the increasing pebble diameter. Therefore, the diameter of pebble impacts the heat transfer and flow performance at the same time. It is desirable to find an optimal pebble diameter according to different reactor design requirements which can balance heat transfer and pressure drop performance.

These results may be a useful reference for further understanding of thermal hydraulic characteristics and the optimum design of fuel spheres in PBR.

## Nomenclature

| | |
|---|---|
| AFPR | Atoms for Peace Reactor |
| BCC | Body-centered Cubic |
| CFD | Computational Fluid Dynamics |
| FCC | Face-centered Cubic |
| Nu | Nusselt Number |
| PBR | Pebble Bed Reactor |
| PNNL | Pacific Northwest National Laboratory |
| SC | Simple Cubic |

## References

[1] GUARDO, A., COUSSIRAT, M., and LARRAYOZ, M.A., *et al.*: Influence of the turbulence model in CFD modeling of wall-to-fluid heat transfer in packed beds, Chemical Engineering Science,2005, 60:1733–1742.

[2] FERRG, YM., and LIN, KY.: Investigating effects of BCC and FCC arrangements on flow and heat transfer characteristics in pebbles through CFD methodology, 2013, Nuclear Engineering and Design 258: 66–75.

[3] NIJEMEISLAND, M., and DIXON, A.G.: Comparison of CFD simulations to experiment for convective heat transfer in a gas-solid fixed bed. 2001, Chemical Engineering Journal, 82: 231–246.

[4] GUARDO, A., COUSSIRAT, M., LARRAYOZ, M.A., RECASENS, F., and EGUSQUIZA, E.: CFD flow and heat transfer in nonregular packing forms for fixed bed equipment design, 2004, Industrial & Engineering Chemical Research. 43, 7049–7056.

[5] EPPINGER, T., SEIDLER, K., and KRAUME, M.: DEM-CFD simulations of fixed bed reactors with small tube to particle diameter ratios, 2011, Chemical Engineering Science 166: 324–331.

[6] LEE, J.J., PARK, G.C., KIM, K.Y., and LEE, W.J.: Numerical treatment of pebble contact in the flow and heat transfer analysis of a pebble bed reactor core, 2007, Nuclear Engineering and Design 237: 2183–2196.

[7] DIXON, A.G., NIJEMEISLAND, M., and STITT, E.H.: Systematic mesh development for3D CFD simulation of

fixed beds: contact points study, 2013 Computer & Chemical Engineering 48: 135–153.

[8] OKAWARA, S., KUROKI, M., STREET, D., and OGAWA, K.: High-fidelity DEM-CFD modeling of packed bed reactors for process intensification, Proceedings of European Congress of Chemical Engineering, Copenhagen,2007.

[9] Pacific Northwest National Laboratory: A New Innovative Spherical Cermet Nuclear Fuel Element to Achieve an Ultra-Long Core Life for use in Grid-Appropriate LWRs, PNNL–16647, 2007.

[10] Nuclear Safety Standards Commission (KTA), KTA 3102.2 Reactor Core Design of High-Temperature Gas-Cooled Reactors. Part 2: Heat Transfer in Spherical Fuel Elements, 1983.